Peripheral (not central) corneal epithelia contribute to the closure of an annular debridement injury

Mijeong Park[a], Alexander Richardson[a], Elvis Pandzic[b], Erwin P. Lobo[c], J. Guy Lyons[d,e,f], and Nick Di Girolamo[a,1]

[a]Mechanisms of Disease and Translational Research, School of Medical Sciences, Faculty of Medicine, University of NSW, NSW 2052 Sydney, Australia; [b]Biomedical Imaging Facility, Mark Wainwright Analytical Centre, Lowy Cancer Research, University of NSW, NSW 2052 Sydney, Australia; [c]School of Mathematics and Statistics, Faculty of Science, University of Sydney, NSW 2006 Sydney, Australia; [d]Discipline of Dermatology, Bosch Institute, Charles Perkins Centre, University of Sydney, NSW 2006 Sydney, Australia; [e]Immune Imaging, Centenary Institute, Royal Prince Alfred Hospital, NSW 2050 Sydney, Australia; and [f]Cancer Services, Royal Prince Alfred Hospital, NSW 2050 Sydney, Australia

Edited by Albert Jun, Johns Hopkins Medicine, Baltimore, MD, and accepted by Editorial Board Member Jeremy Nathans November 14, 2019 (received for review July 17, 2019)

Corneal epithelia have limited self-renewal and therefore reparative capacity. They are continuously replaced by transient amplifying cells which spawn from stem cells and migrate from the periphery. Because this view has recently been challenged, our goal was to resolve the conflict by giving mice annular injuries in different locations within the corneolimbal epithelium, then spatiotemporally fate-mapping cell behavior during healing. Under these conditions, elevated proliferation was observed in the periphery but not the center, and wounds predominantly resolved by centripetally migrating limbal epithelia. After wound closure, the central corneal epithelium was completely replaced by K14$^+$ limbal-derived clones, an observation supported by high-resolution fluorescence imaging of genetically marked cells in organ-cultured corneas and via computational modeling. These results solidify the essential role of K14$^+$ limbal epithelial stem cells for wound healing and refute the notion that stem cells exist within the central cornea and that their progeny have the capacity to migrate centrifugally.

limbal epithelial stem cells | K14CreERT2-Confetti mice | corneal wound healing | spatiotemporal image correlation spectroscopy | computational modeling

Limbal epithelial stem cells (LESCs) play a key role in corneal homeostasis (1–3) and wound healing (4–6). These cells are thought to reside in the outskirts of the cornea, in a region known as the limbus. LESCs are typically stationary, undifferentiated, and slow-cycling, yet are highly proliferative when activated and are able to divide symmetrically and asymmetrically to produce daughter stem cells (SCs) or transit amplifying cells (TACs) (5, 7–9). TACs have high but limited proliferative potential and are motile because they must replace terminally differentiated cells (TDCs) which are constantly sloughed from the ocular surface. The long-held belief is that this dynamic process maintains tissue mass, and is in agreement with the XYZ hypothesis (2). Following injury, LESCs and/or their early progeny ramp their proliferation, forcing TACs to move faster in order to seal the wound in a timely manner (5, 6, 10).

It is generally accepted that central corneal epithelia have limited self-renewal and therefore poor regenerative capacity (11). However, this well-entrenched dogma (4, 12, 13) has been challenged. Firstly, Dua and colleagues (14) found persistent islands of healthy corneal epithelia in patients with limbal stem cell deficiency (LSCD); an intriguing observation given the clinical absence of an intact limbus. Secondly, a controversial study (15) concluded that; 1) the limbus does not contribute to the steady-state corneal renewal because transplanted limbal epithelia did not migrate centripetally, 2) mouse central cornea could be serially transplanted into the limbal region of a recipient mouse to regenerate the cornea, 3) the cornea remained transparent after cauterizing the limbal circumference to destroy the limbal epithelium and underlying stroma, and 4) corneal epithelia from different species (except calf and human) contain SCs because they formed large holoclone-like colonies. Despite these findings, inconsistencies associated with this hypothesis have been highlighted (16); nonetheless, this concept is semisupported by recent work of Nasser and coauthors who showed that upon removing the mouse limbus, cornea-committed epithelia could de-differentiated into LESC and travel in the opposite direction (i.e., centrifugally) to repopulate the SC pool and reestablish the tissue boundary (17). It should be noted, however, that the fate-mapping exercise conducted to acquire these interesting data was based on K15, which may or may not be an ideal marker for these cells (18). Similarly, in short-term human organ culture, laser-ablating the limbus while sparing the central cornea (otherwise described as a doughnut-shaped or annular wound), triggered reepithelialization from both directions, notably faster centrifugally and explained by elevated proliferation in the center (19).

Overall, these observations suggest that the epithelium in the center can maintain the cornea in the absence of LESCs. This then raises the possibility of the existence of SCs within the central cornea which are activated upon injury. However, methods for real-time monitoring to unequivocally visualize and identify which cells take part in this process are scant. In order to resolve these conflicting theories, multicolored Confetti reporter mice were given various annular debridement injuries that either impacted the limbus or the peripheral cornea but spared the central region. Herein, we provide real-time spatial-temporal recordings of how LESCs and their progeny contribute to the initial phase of annular wound repair by visualizing the predominant unidirectional (centripetal) clonal movement into the wound bed. In contrast, centrally

Significance

The well-accepted proposition that central corneal epithelia have limited self-renewal and therefore poor regenerative capacity has recently been challenged. However, methods for real-time monitoring to identify which cells take part in this process are scant. In this study, we visualized and quantified the contribution of central versus peripheral/limbal epithelia during annular wound healing by intravital imaging, through an organ culture system, and via computational modeling. Our results verify the contribution of K14$^+$ limbal-derived stem cells and their early progeny in playing a vital role in this process, while central corneal epithelia contribute minimally to wound closure.

Author contributions: M.P. and N.D.G. designed research; M.P., A.R., E.P., E.P.L., and J.G.L. performed research; M.P. and N.D.G. contributed new reagents/analytic tools; M.P., A.R., E.P., E.P.L., and J.G.L. analyzed data; and M.P., A.R., E.P., E.P.L., J.G.L., and N.D.G. wrote the paper.

The authors declare no competing interest.

This article is a PNAS Direct Submission. A.J. is a guest editor invited by the Editorial Board.

[1]To whom correspondence may be addressed. Email: n.digirolamo@unsw.edu.au.

This article contains supporting information online at https://www.pnas.org/lookup/suppl/doi:10.1073/pnas.1912260116/-/DCSupplemental.

First published December 16, 2019.

located epithelia were minimally displaced in the centrifugal direction, and therefore did not partake in reepithelialization. Our results provide a clearer understanding of corneal epithelial regeneration and demonstrate the essential role of limbal-derived SCs in injury repair.

Results

Contribution of Limbal/Peripheral Versus Central Corneal Epithelia in Wound Resolution. To confirm the extent of epithelial debridement, mice were euthanized before, just after, and during the early stages of wound healing and corneas were examined after staining sections with Periodic Acid-Schiff (PAS) (Fig. 1). Mice which endured a type I annular wound displayed no peripheral epithelium in the injured zone; however, the central, paracentral, and limbal epithelium remained intact (Fig. 1 *A* and *B*, first column and Fig. 1*C*, first row) compared to the uninjured control (Fig. 1 *A* and *B*, second column and Fig. 1*C*, third row). At 24 h postinjury, the peripheral cornea was covered by 1 to 2 layers of epithelia, and mild stromal inflammation was observed (Fig. 1 *C*, *Middle* row). Notably, central corneal epithelial thickness was diminished, and basal epithelia that covered the defect after 24 h were morphologically similar to wing cells from uninjured corneas, indicating that both central and peripheral epithelia may have migrated to cover the defect.

In Vivo and Ex Vivo Wound Resolution by Moving Peripheral and Central Corneal Epithelia. Next, we used wild-type (WT) and Confetti mice to more accurately measure the contribution of centripetal versus centrifugal migration during corneal wound healing (Fig. 2). Notably, in this set of experiments older mice were used, allowing us to deliver a slightly larger (type II) epithelial abrasion. In WT mice, fluorescein staining (after 8 h) revealed that centripetal movement was significantly faster than centrifugal displacement (7.5 ± 3.1 μm/h vs. 1.5 ± 0.2 μm/h, $P = 0.011$) (Fig. 2 *A* and *B*). To confirm these results with a more sophisticated visual

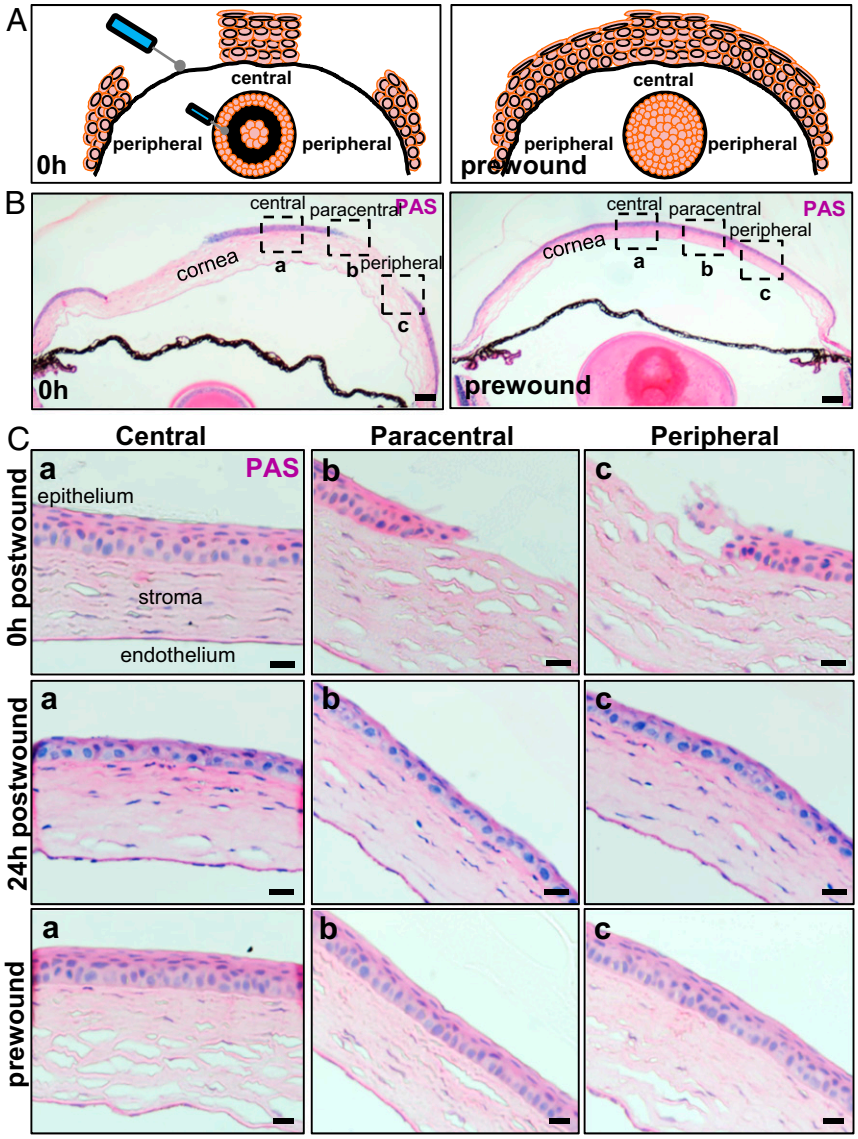

Fig. 1. Corneal epithelial restoration after an annular debridement injury. (*A*) Schematic depiction on how the annular epithelial wound was inflicted. (*B*) WT mice ($n = 4$/group/time-point) had their right corneal epithelium mechanically debrided to inflict a type I annular defect. Representative images of transverse sections stained with PAS provide a panoramic overview of tissue architecture immediately after (*Left*) and prior to (*Right*) wounding. (Scale bars, 200 μm.) (*C*) The region encompassed by the hatched squares in *B* is magnified in (*a*) central, (*b*) paracentral, and (*c*) peripheral zones, respectively. Displayed are representative images taken immediately after wounding (first row), 24 h postwounding (second row), and prior to injury (third row). (Scale bars, 20 μm.)

tool, Confetti mice of identical age and with a complete streaking pattern (~30-wk posttamoxifen), were given the same injury, then analyzed (Fig. 2*C*). Both centripetal and centrifugal displacement of multicolored fluorescent clones was readily detected at 8 h, and wounds were sealed by 24 h postinjury. In line with data from WT mice, centripetal migration of $K14^+$ Confetti-derived streaks was faster than centrifugal motion (11.76 ± 6.1 μm/h vs. 4.32 ± 4.9 μm/h, $P = 0.048$) (Fig. 2*D*). Using intravital (Fig. 2*E*, first and second panels) and confocal (Fig. 2*E*, third panel) microscopy, it was also apparent that 48 h after wounding, colored clones were often disconnected from their original colony (Fig. 2*E*, second and third panels, arrows).

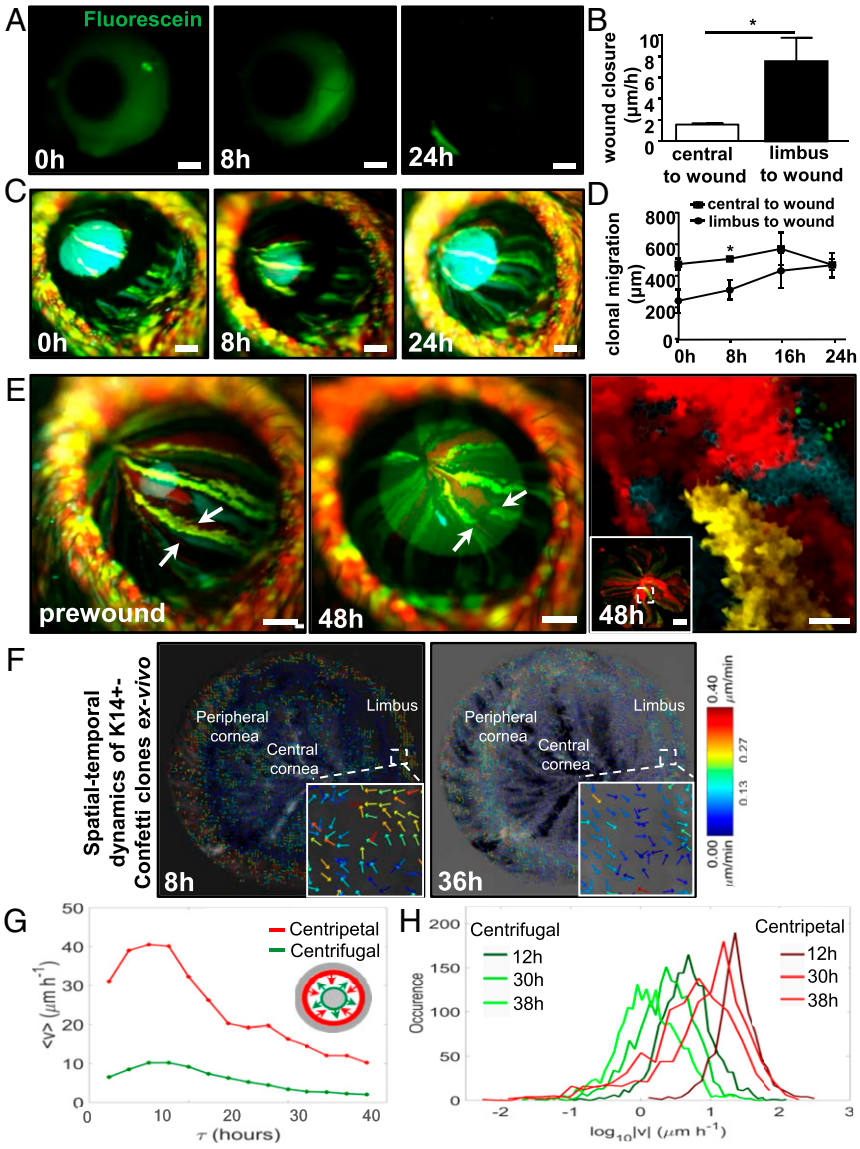

Fig. 2. Centripetal verses centrifugal migration. See also Movies S1 and S2. (*A*) Corneas of live WT mice ($n = 4$/group) were monitored by applying sodium fluorescein (green) at 0, 8, and 24 h post a type II annular wound. (Scale bars, 400 μm.) (*B*) In vivo wound-closure rate in WT mouse corneas following a type II annular wound, comparing centripetal (limbus-to-wound) to centrifugal (central-to-wound) velocity (mean ± SD, $n = 4$/group, $^*P < 0.05$, unpaired 2-tailed Welch's *t* test). (*C*) In vivo monitoring of clonal streaks in Confetti transgenic mice ($n = 3$/group). Displayed are images taken at 0, 8, and 24 h post a type II annular injury. (Scale bars, 400 μm.) (*D*) In vivo Confetti streak displacement postannular wounding, comparing centripetal (limbus-to-wound) to centrifugal (central-to-wound) velocity (mean ± SD, $n = 3$/group, $^*P < 0.05$, unpaired 2-tailed Welch's *t* test). (*E*) Confetti streaks were imaged in vivo before (prewound, first panel) and 48 h after injury (second panel). Arrows point to the same region. (Scale bars, 400 μm.) The same corneas were flat-mounted and viewed by confocal microscopy (third panel). The region encompassed by the hatched square (*Inset*) is magnified. (Scale bars, 100 μm and 500 μm [*Inset*].) (*F*) Eyes from Confetti mice ($n = 4$) were enucleated immediately after a type II wound, placed in organ culture, and imaged by light-sheet microscopy every 2 h for 48 h. STICS was applied on a time series of 2D maximum intensity projections of 3D image stacks. Vector flow-maps were generated after correcting for corneal curvature; each represent migration and direction of clone movement from images taken at 8 and 36 h, respectively. *Insets* are magnified views of a representative region encompassed by the small hatched square to show the multidirectional movement of groups of cells within a clone, depicted as colored arrows with an associated heat-map which acts as a speed gauge. (*G*) Ex vivo Confetti streak displacement following a type II annular wound, comparing centripetal (limbus-to-wound, red) to centrifugal (central-to-wound, green) velocity. The speed of fluorescent clones from 0 to 40 h for a representative cornea is displayed. A schematic representation of an annular wound is also included. Here, arrows are color-coded with the line graphs in the main panel to indicate the direction of wound closure. The gray area represents intact epithelia. (*H*) Ex vivo Confetti clone speed at representative time points of 12, 30, and 38 h postwound is displayed by individually colored histogram (centrifugal migration, dark to light green; centripetal migration, burgundy to red).

These in vivo results are supported by those generated in ex vivo organ-cultured corneas (Movies S1 and S2 and Fig. 2 *F* and *G*). To this end, Spatiotemporal Image Correlation Spectroscopy (STICS) analysis (6) was applied to more accurately map the spatial-temporal dynamics of K14$^+$-Confetti cells within clones in organ-cultured corneas that received a type II annular wound. Notably, after correcting for corneal curvature from the 3-dimensional (3D) image stacks and the frequency at which corneas could be monitored, the velocity and direction of migrating clones were determined with greater precision during wound closure. In this ex vivo paradigm, K14$^+$-Confetti clones acquired both centripetal and centrifugal motion (Movie S1) similar to their displacement in vivo (Fig. 2 *C* and *E*). At 8 and 36 h postinjury, the direction and velocity of clonal migration were calculated and displayed as vector flow-maps (Fig. 2*F*). This analysis indicated that groups of cells within clones moved in a multidirectional manner (Fig. 2 *F*, *Insets*). The flow-maps (Fig. 2*F* and Movie S2) demonstrated that centripetal movement was faster than centrifugal motion. Centripetal migration from the periphery decelerated from 17.0 ± 13.1 μm/h to 8.1 ± 2.9 μm/h (Fig. 2*G*, red and Fig. 2*H*, burgundy to red) and from 7.4 ± 7.4 μm/h to 6.0 ± 8.4 μm/h in centrifugal direction (Fig. 2*G*, green and Fig. 2*H*, dark to light-green) as wounds closured.

Cells Involved in the Long-Term Maintenance of the Corneal Epithelium after Wound Closure. To visualize how and what cells partake in healing a type II annular wound, corneas of Confetti mice were monitored long-term using intravital microscopy (Fig. 3 *A* and *B*). Extended monitoring demonstrated that the central island and/or the distorted colored streaks (Fig. 2*E*, second and third panels), disappeared as the corneal epithelium was replenished by centripetally migrating K14$^+$-Confetti-derived clones (Fig. 3*A*), suggesting that the corneal epithelium is predominantly

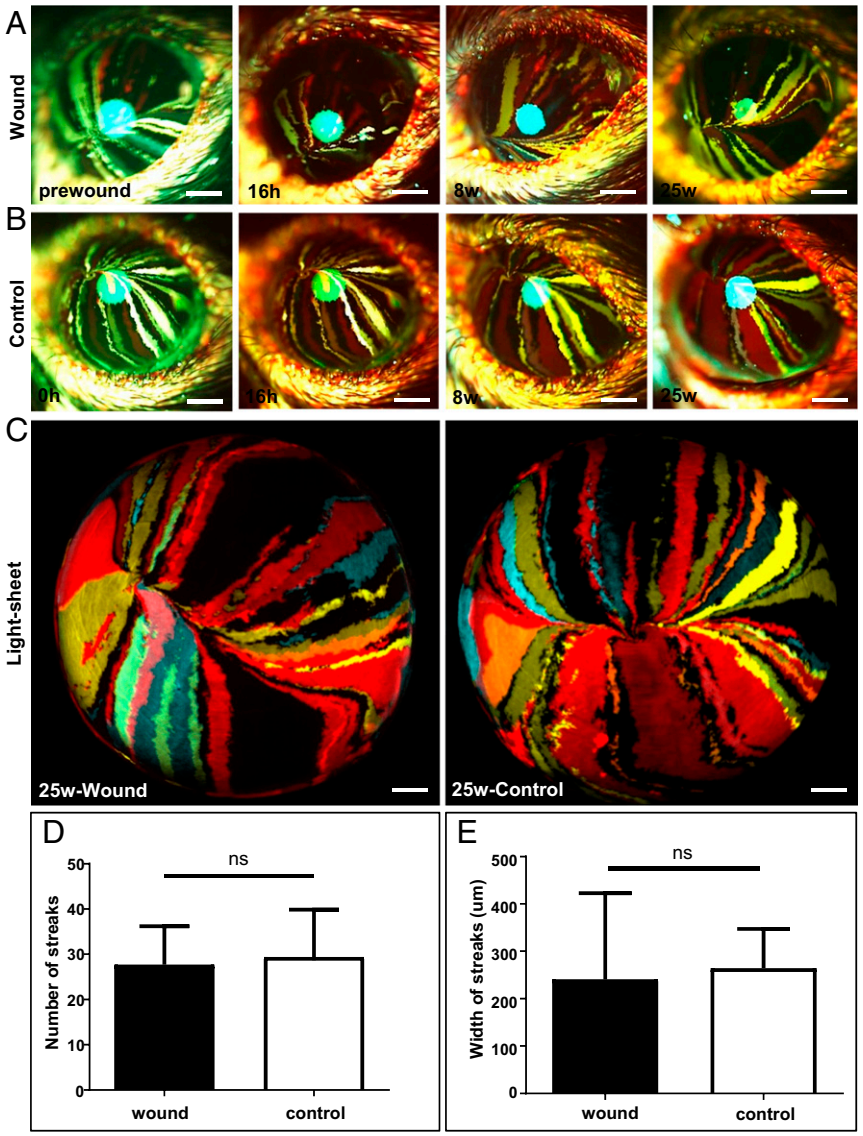

Fig. 3. Cells involved in the long-term maintenance of corneal epithelium after wound closure. (*A*) Confetti mice at 30-wk posttransgene induction ($n = 3$/group) had their right corneal epithelium mechanically debrided to create a type II annular wound, after which they were monitored long-term. Corneas were imaged by intravital microscopy before and at 16 h, 8-wk, and 25-wk postinjury. (Scale bars, 400 μm.) (*B*) The intact left eye was used as the control. (Scale bars, 400 μm.) (*C*) A further set of corneas ($n = 3$/*group*) were procured from euthanized mice and imaged by light-sheet microscopy 25-wk after inflicting a type II annular injury. (Scale bars, 500 μm.) (*D* and *E*) Streak number and width (respectively) at 25-wk postinjury (mean ± SD, $n = 3$/group, ns = not significant; $P > 0.05$, unpaired 2-tailed Welch's *t* test).

maintained long-term by limbal/peripheral-derived cells, as opposed to epithelia from the central cornea. Interestingly, there was no visible difference in streak development between injured and uninjured corneas during this prolonged monitoring period (Fig. 3 *A*–*C*). The number of clonal streaks that developed at 25-wk postwounding compared to control corneas was 27.7 ± 8.5 vs. 29.3 ± 11.2; $P = 0.85$ (Fig. 3*D*) and their width measured 240.6 ± 182.0 μm vs. 264.3 ± 83.1 μm; $P = 0.85$ (Fig. 3*E*), respectively, suggesting that there was no dramatic change in SC activity that influenced the frequency of symmetric and/or asymmetric division (3, 5, 6) after delivering such minor injuries.

Central Corneal Epithelia Contribute Minimally to Wound Healing. Similar to the data obtained from older Confetti mice with fluorescent streaks within their central cornea (Figs. 2 and 3), in young mice that received a type I annular injury, the central island (which typically harbors fluorescent patches) disappeared as the corneal epithelium was replaced by centripetally migrating $K14^+$-Confetti-derived clones (Fig. 4*A*). At 1-wk posttransgene

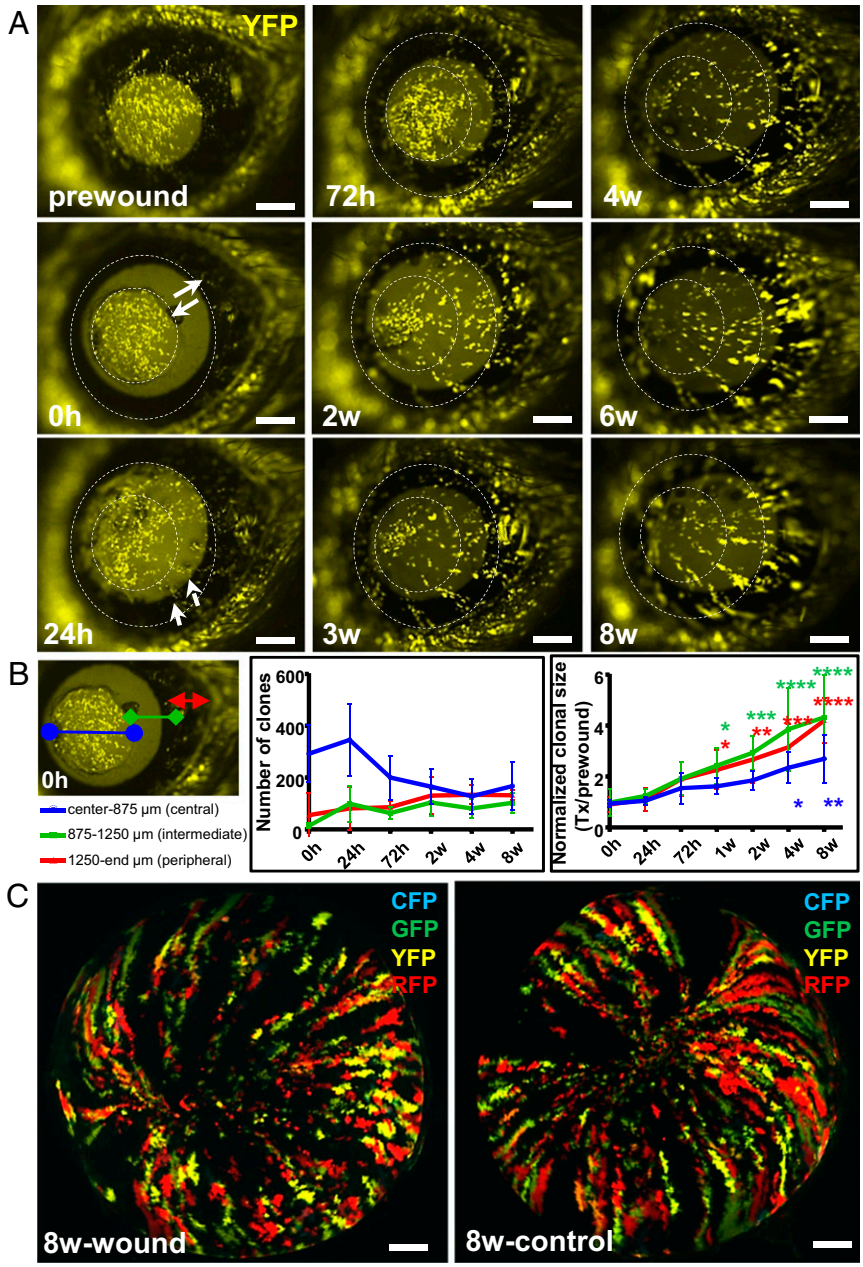

Fig. 4. Reepithelialization of annular wounds by centripetally migrating $K14^+$ limbal-derived clones. (*A*) One week after transgene induction, Confetti mice ($n = 5$/group) had their right corneal epithelium mechanically debrided to create a type I annular wound. For ease of visualization, only YFP^+ (yellow) luminescing cells were monitored long-term by intravital microscopy. Solid white arrows indicate the wound span immediately (0 h) after injury. Small white arrows point to peripheral YFP^+ clones moving centripetally across the wound bed 24 h postinjury. Hatched white circles indicate the wounded region. (Scale bars, 400 μm.) (*B*) YFP^+ patches and clones located in the central (apex-to-875 μm, blue), intermediate (875 μm-to-1250 μm, green), and peripheral (1250 μm-to-eyelid margin, red) zones were analyzed, and their number and size displayed. Data represent mean ± SD, $n = 5$/group, $^*P < 0.05$, $^{**}P < 0.01$, $^{***}P < 0.001$, $^{****}P < 0.0001$, 2-way ANOVA with Dunnett's multiple comparisons test. (*C*) After enucleation, the same corneas and their contralateral control counterparts were imaged by light-sheet microscopy at 8-wk postinjury. (Scale bars, 500 μm.)

induction, small K14$^+$ patches of fluorescing cells were detected across the cornea (Fig. 4*A*, column 1, first panel). Notably, only the yellow channel was displayed, since cells could be readily discerned on a dark background (Fig. 4*A*, column 1, second panel). Within 24 h of wounding, the debrided zone displayed evidence of emigrating yellow clones (Fig. 4*A*, column 1, third panel, small white arrows) which emerged from K14$^+$-Confetti limbal epithelia. Interestingly, yellow fluorescent protein (YFP)$^+$ patches within the intact central island remained relatively stationary (Fig. 4*A*, column 1, third panel), and with time, the size and the amount of fluorescence within this region was reduced over the ensuing 3-wk (Fig. 4*A*, column 2, third panel), then disappeared after 4-wk as the region was replaced by new limbal-derived K14$^+$-Confetti clones (Fig. 4*A*, column 3).

Next, cells involved in resurfacing these wounds were quantified. The strategy here was to divide the cornea into specific zones including center (apex-to-875 μm), intermediate (875 μm-to-1250 μm) and periphery (1250 μm-to-eyelid edge) to ascertain the contribution of YFP$^+$ central patches versus limbal-emerging clones over time (Fig. 4*B*, first panel). The number of fluorescent patches in the central zone decreased from 345.6 ± 139.1 to 167.6 ± 92.1, while clones in the intermediate and peripheral zones gradually increased from 99.4 ± 69.0 to 102.4 ± 40.3 and 81.4 ± 83.1 to 132.0 ± 20.1, respectively, after wound closure from 24 h to 8-wk postinjury (center vs. intermediate; $P < 0.0001$, center vs. periphery; $P < 0.0001$ and intermediate vs. periphery; $P = 0.32$, respectively) (Fig. 4*B*, second panel). Concurrently, the size of YFP$^+$ patches and clones across the cornea increased with time (Fig. 4*B*, third panel). Statistically significant results were noted much earlier (i.e., 1-wk

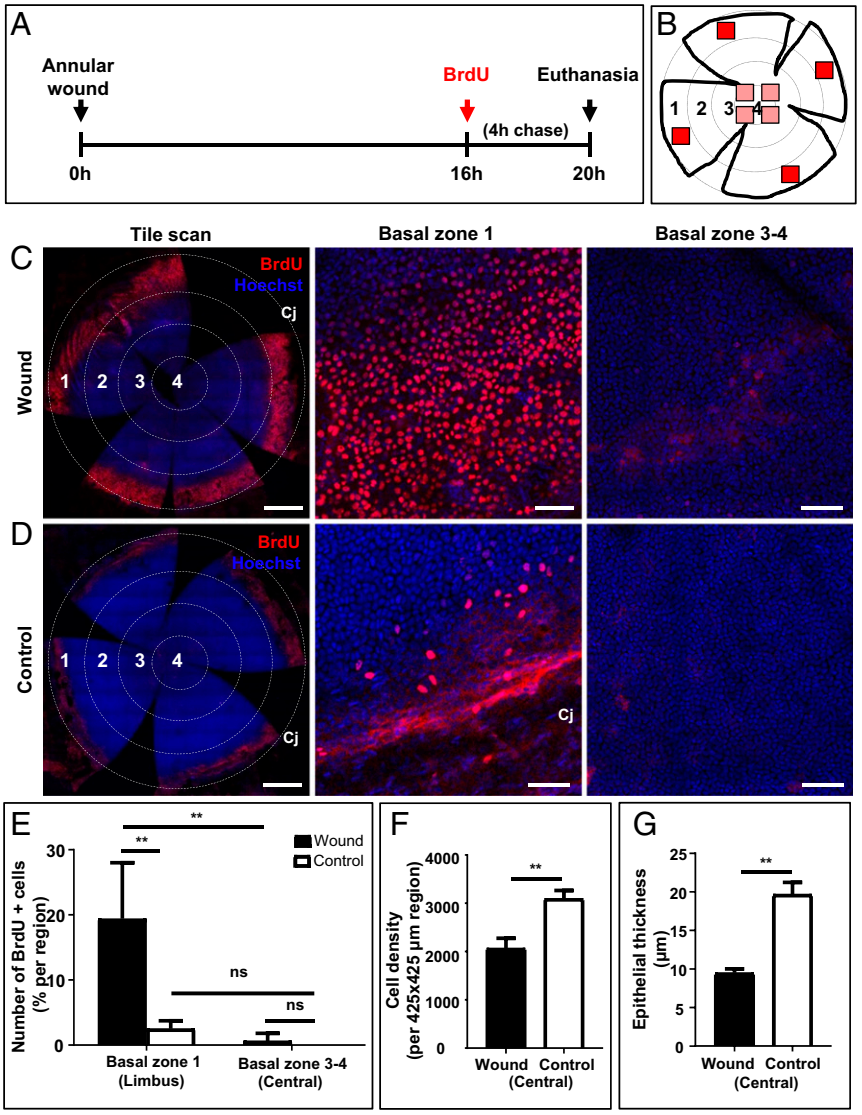

Fig. 5. Proliferation of peripheral and central corneal epithelia after an annular injury. (*A*) Schematic diagram shows the experimental design whereby WT mice ($n = 4$/group) had their right corneal epithelium debrided to generate a type II annular wound. After 16 h, mice were injected with BrdU, euthanized 4 h later, then corneas were procured and flat-mounted. (*B*) Schematic diagram shows a flattened cornea in which 4 equally distant concentric rings are drawn, and zones numbered accordingly; 1 (limbus), 2 (peripheral), 3 (paracentral), and 4 (central). BrdU$^+$ basal epithelia within zone 1 and zones 3 and 4 were counted in each of 4 randomly selected regions that measured 425 × 425 μm in area (red squares). (*C* and *D*) Representative confocal images of wounded and control corneas stained for BrdU (red) and counterstained with Hoechst (blue). (Scale bars, 500 μm [tile scan] and 100 μm [basal layer of zones 1, and 3, and 4].) (*E–G*) Bars in the graphs represent percentage BrdU$^+$ basal epithelia in zone 1 (limbal) compared to zones 3 and 4 (paracentral and central), and basal cell density and epithelial thickness within the intact central epithelial island comparing wounded to controls (mean ± SD; $n = 4$/group independent corneas, $^{**}P < 0.01$, 2-way ANOVA with Tukey's multiple comparisons; ns = not significant).

after injury) for the intermediate and peripheral clones (0 h vs. 1-wk; $P = 0.021$ and $P = 0.035$, respectively) and later (>4-wk) in the center (0 h vs. 4-wk; $P = 0.029$ and 0 h vs. 8-wk; $P = 0.003$). These data suggest that central corneal epithelial cells contributed minimally to annular wound healing since they were replaced by centripetally migrating limbal-derived epithelia (Fig. 4*A*). At 8-wk postwounding, corneas of euthanized mice were imaged by light-sheet microscopy to show that the Confetti striping pattern was restored without a concomitant increase in clone number or clonal expansion compared to contralateral control eyes (Fig. 4*C*), again implying that LESC activity was minimally impacted under these conditions.

Elevated Proliferation in Peripheral Basal Epithelia Potentially Contributes to Wound Closure. To determine how limbal and/or peripheral epithelia partake in resolving annular injuries, cell proliferation was assessed by BrdU labeling just prior to the closure of a type II wound (Fig. 5*A*). In this experiment, 4 randomly selected regions within 4 numerically defined concentric zones were imaged

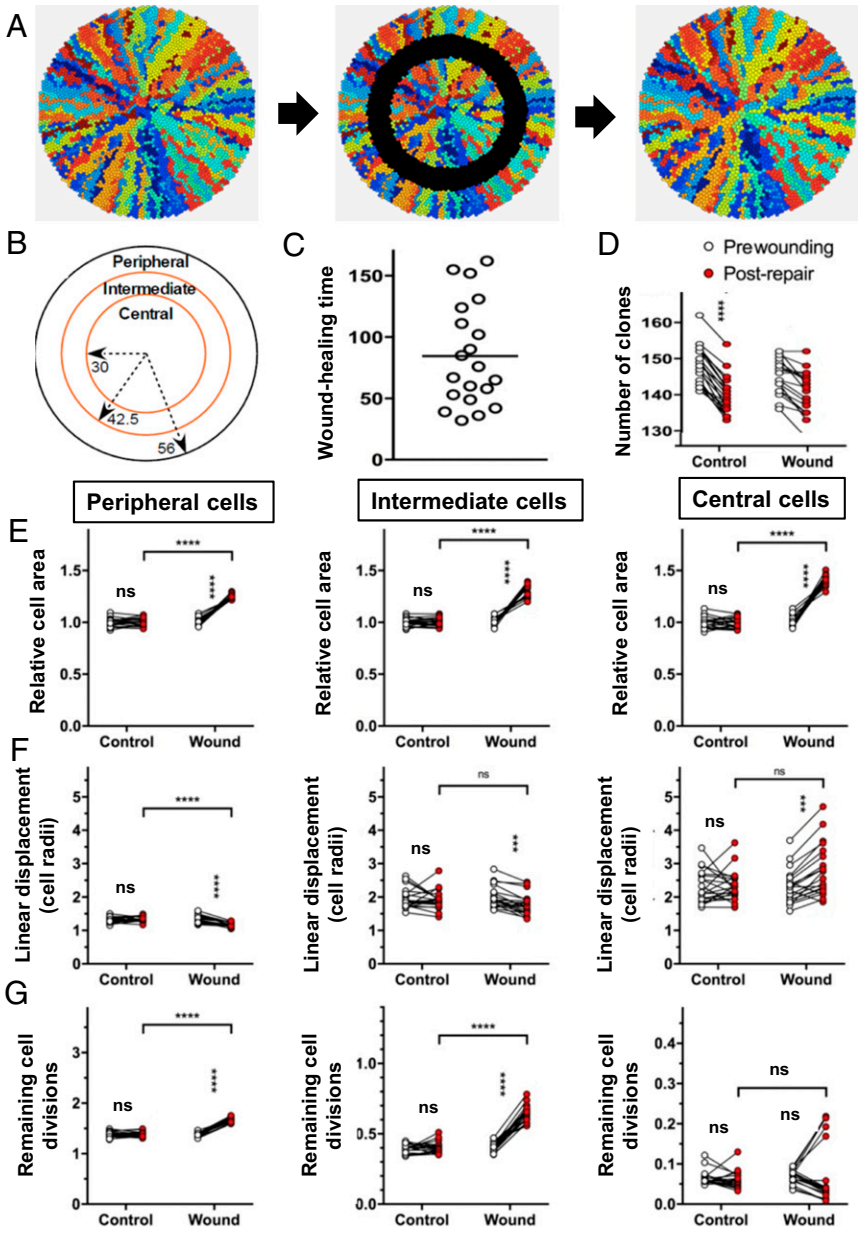

Fig. 6. Computational modeling to investigate the effect of wounding on the composition and structure of the repaired corneal epithelium. See also Movie S3 and Table 1. (*A*) Examples of simulated corneas immediately before, during, and immediately after wound repair (left to right, respectively). (*B*) Wounds were made by removing epithelial cells from an intermediate zone, i.e., between 42.5 and 30 cell radii from the center. (*C*) Cell properties were measured in these regions and in the peripheral zone. Wounds were completely repaired in less than 200-time steps. (*D*) Clone number was counted prewounding and postrepair. (*E*) Cell size was measured for all cells in each zone immediately before wounding and immediately after healing was complete or, in the case of unwounded corneas, at t = 2300 ("prewounding") and t = 2500 ("postwounding"). Cell size was adjusted for differences in prewounding size, which varied in the 3 zones. The mean cell area is plotted for each cornea in the peripheral, intermediate, and central zone. (*F*) The mean linear displacement, a measure of clonal dispersion, was determined for all cells in the peripheral, intermediate, and central zones, as indicated below the X-axis. (*G*) TAC (n), the number of remaining cell divisions of the TACs in corneas was determined for all cells in the peripheral, intermediate, and central zones, as indicated below the X-axis. Data (*D*–*G*) represent mean ± SD, $n = 20$/group, ***$P < 0.001$, ****$P < 0.0001$, ns (not significant) = $P > 0.05$ by repeated measures (2300-time unit) one-way ANOVA with Sidak's multiple comparisons correction.

(Fig. 5*B*). Minimum proliferation was detected in zone 2, which harbored the wound and contained migratory epithelia (Fig. 5*C*, first column). Thus, only the limbal/peripheral region (zone 1) was compared to the paracentral and central regions (i.e., zones 3 and 4) for proliferative activity. At 20 h postwounding, the number of $BrdU^+$ basal epithelia increased within the limbal/peripheral region (Fig. 5*C*, zone 1) compared to the paracentral and central regions (Fig. 5*C*, zones 3 and 4). This contrasted with the appearance of fewer $BrdU^+$ basal epithelia in the contralateral uninjured eye, irrespective of the zone that was assessed (Fig. 5*D*). Basal cell proliferation in the periphery increased by 7.6-fold compared to uninjured corneas (19.8 ± 8.6% vs. 2.6 ± 1.1%, $P = 0.0084$), while minimal proliferation was detected within the central island of epithelia adjacent to the injury site (Fig. 5*E*). Interestingly, basal cell density (Fig. 5*F*) and epithelial thickness (Fig. 5*G*) significantly decreased within the intact central epithelial island, a result that was congruent with the histology (Fig. 1*C*). Therefore, under these conditions, central corneal epithelia do not proliferate and only contributed to wound closure by altering their size and shape.

Computational Modeling of Corneal Epithelial Wound Healing after an Annular Injury. Using computational modeling, we previously showed that population density-driven pressure is sufficient to promote centripetal LESC-derived clonal migration after ultraviolet (UV) irradiation exposure (5) and following a 2 mm central epithelial debridement wound (6). To determine whether the same forces play a role in the cellular responses triggered during annular wound repair, we adapted our mathematical model to incorporate a similar injury scenario (Fig. 6). Annular wounds equivalent in area were simulated by replacing cells in the intermediate zone with "blank" cells (Fig. 6*A*), which offered minimal resistance to the movement of adjacent epithelia. Simulation conducted under these conditions resulted in corneas healing completely within 200-time steps (Fig. 6*C* and Movie S3). Moreover, there was no difference in the number of clones generated in wounded versus control corneas, or in prewounded compared to postrepaired eyes (Fig. 6*D*). At the end of the healing process, basal epithelial cell size significantly increased in the peripheral, intermediate, and central zones compared to basal cells in control corneas (Table 1 and Fig. 6*E*), results which agree with our in vivo data (Figs. 1–5). Our computational model was also used to examine the effects of wounding on the organization of the corneal epithelium. We quantified the mean linear displacement (5, 6) as a measure of clonal dispersion, and demonstrated that remaining central clones were more disordered in the central zone (Fig. 6*F*), possibly due to relaxed pressure at the outer edge (i.e., adjacent to the injury site). Simulations conducted after wounding indicated migration occurred in both directions, although centripetal movement predominated over time. The initial centrifugal surge by cells in the central zone was primarily due to an increase in cell size, likely induced by pressure relief from the absence of abutting cells, as replication was not increased in this region after wounding in contrast to that which transpired in the peripheral and intermediate zones (Fig. 6*G*).

Table 1. Average size of basal epithelia from simulated corneas, related to Fig. 6 and Movie S3

Relative to cell areas	Peripheral cells	Intermediate cells	Central cells
Wound	1.2 ± 0.02	1.32 ± 0.06	1.41 ± 0.05
Control	1.0 ± 0.03	1.0 ± 0.04	1.0 ± 0.05
P value	<0.0001 (****)	<0.0001 (****)	<0.0001 (****)

The average size of the basal cells in peripheral, intermediate, and central areas from simulated corneas was significantly increased in annular wounds. Data represent mean ± SD, $n = 20$/group, ****$P < 0.0001$ by repeated measures (2300-time unit) one-way ANOVA with Sidak's multiple comparisons correction.

How Does Wound Healing Proceed in the Absence of LESCs? To determine whether the central corneal epithelium alone has enough regenerative activity to resolve an annular injury and reinvigorate the corneal epithelium to a healthy state, the entire limbal/peripheral epithelial annulus was debrided in a 360-degree manner (*SI Appendix*, Fig. S1*A*; a type III wound). After the injury, eyes became opaque (*SI Appendix*, Fig. S1*B*; second panel), and PAS^+ goblet cells and $CD31^+$ blood vessels (*SI Appendix*, Fig. S1 *C* and *D*, respectively) encroached from the periphery. During the healing process, several interesting phenomena were noted regarding the intact central island of epithelia. In some mice, it remained a collective of $K12^+$ cells (*SI Appendix*, Fig. S1*D*; second panel), in others, it became fragmented into several microclusters of $K12^+$ epithelial cells (*SI Appendix*, Fig. S1*D*; third panel), or it disappeared (*SI Appendix*, Fig. S1*E*; fourth panel) and was rapidly replaced by conjunctival epithelia (*SI Appendix*, Fig. S1*E*; fifth and sixth panels).

Discussion

The wounds our mice received were symmetrical, shallow, and rapid to resolve; nonetheless, they were ideal for interrogating hypotheses that have challenged the status quo in recent times, including whether small corneal epithelial debridement wounds resolve by centripetal or centrifugal migration, whether SCs or early TACs are actively involved in the initial phase of reepithelialization, and if so, whether this dynamic activity can be visualized, measured, and modeled, and the importance of an intact limbus in maintaining a healthy corneal epithelium. In summarizing the data accrued from this investigation, we formulated a working model (Fig. 7) whereby debriding the epithelium between the peripheral and paracentral cornea, leaving behind an intact limbal and central epithelium (Fig. 7*A*), induced proliferation in the periphery (but not the central cornea). This elevated proliferative activity entices new basal epithelia to travel into the wound bed in a centripetal manner. In contrast, cells at the edge of the central epithelial island move minimally; any measurable motion due to changes in cell shape and size (Fig. 7*B*). These wounds typically resolve within 24 h, after which proliferation subsides, and $K14^+$-Confetti-derived clones begin replacing cells within the central epithelial island (Fig. 7*C*) until this region is completely remodeled (Fig. 7*D*) and tissue mass and function are restored to steady-state levels.

Humans have evolved intricate microstructures within the limbus known as the Palisades of Vogt (20) which circumscribe the cornea and harbor epithelial SCs. Their concertina-like arrangement increases surface area, allowing more SCs to be housed within a confined space, and provides protection from external insults. These structures are absent in mouse, instead the same region tapers into a few epithelial layers which are protected by the eyelids. The mouse corneal epithelium is thickest in the center; therefore, if SCs exist in this location, they would be shielded by the extra layers. Irrespective of their location (i.e., peripheral or central), it is widely accepted that epithelial SCs of the mammalian cornea are found in a basal location (21, 22) and held in a primitive, quiescent state to ensure their longevity. The SC niche is therefore a place where nutritional, stemness, immunological, and damage-associated signals are accessible; logically this should be nearest a vascular supply, which in the healthy cornea is in the periphery. To this end, there has been ongoing debate as to the existence of central-corneal versus limbal-located epithelial SCs (CESC vs. LESC) (23). The CESC hypothesis accepts that SCs exist in the limbus but are only active after injury (15). In support of this proposition, several reports have demonstrated persistent islands of "normal" corneal epithelia in patients with total LSCD (14), and in one such case this resulted in complete self-repair of the corneal surface (24). If indeed CESCs exist and are only active upon wounding, then in our study, BrdU-stained cells should have

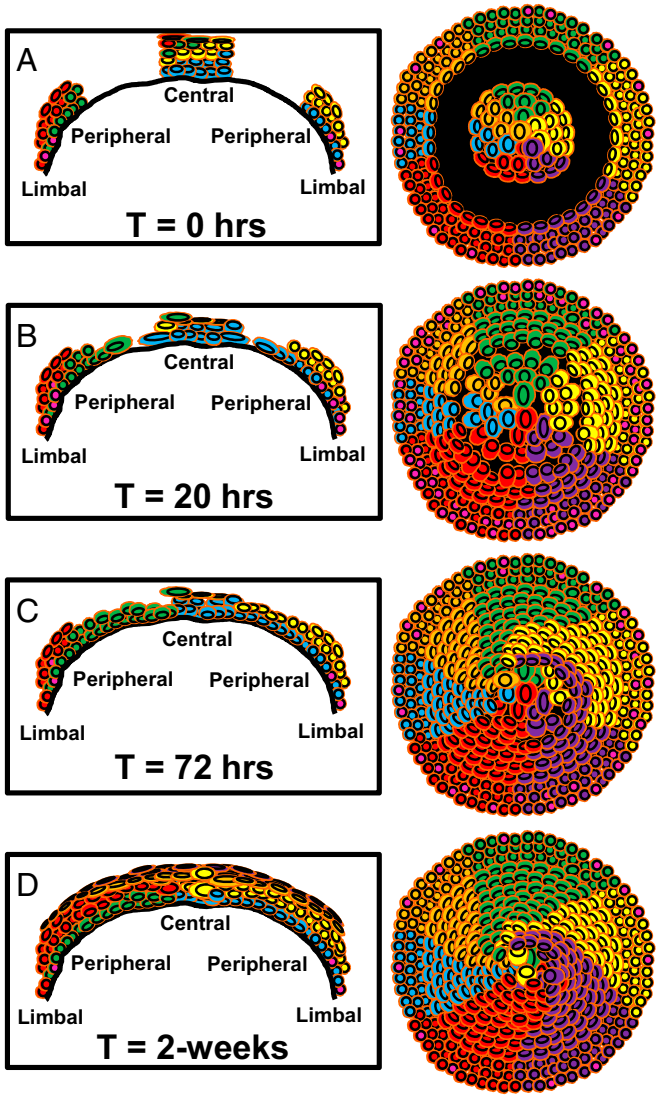

Fig. 7. Schematic representation of how annular epithelial wounds heal. The model is based on results obtained from Confetti mouse corneas where $K14^+$ LESC-derived clones are distinguishable as multicolored colonies that form curvilinear stripes. The first column is a cross-sectional view of the cornea spanning limbus-to-limbus. The second column provides an overview of the entire cornea from an apical perspective. Each row (*A–D*) corresponds to a specific time point after injury. (*A*) Time (T) = 0 h; represents the time when corneas are debrided to inflict an annular wound (black region). (*B*) T = 20 h; proliferation in the limbus increases (pink nuclei) and cells move into the wound bed from the periphery. Cells at the advancing edge are flatter and larger. Cells on the fringe of the central island do not proliferate or move, rather they change shape due to the extra space available. This shape change coincides with a thinner corneal epithelium within the central island. (*C*) T = 72 h; proliferation subsides, and epithelial cells have filled in the void. They begin stratifying and replacing cells from the central island. (*D*) T = 2-wk; epithelial layering is restored and only a few of the original central epithelial cells remain.

been detected within the uninjured central epithelial island. However, this was not the case; instead proliferation was elevated in the limbal/peripheral region of the wounded eye (Fig. 5), which likely contributed to the centripetal surge of basal cells into the deepithelialized zone (Figs. 2–4 and Movies S1–S3). Certainly, this is supported by our computational model, which demonstrates that wounded corneas have the same basic properties as unwounded corneas (motility in response to pressure, location of stem cells in the limbus, and limited proliferative potential of transit amplifying cells) accurately simulate the healing of annular wounds seen in vivo. This is consistent with the ability to rapidly heal wounds being an innate property of the corneal epithelium, requiring only an increase in proliferation in response to the reduced population pressure caused by removal of the epithelium at the wound site, and not requiring the activation of a latent SC population in the cornea. These results are, however, at odds with those of Sandvig and coworkers who showed that small diameter (1.7 mm) erosions in the rat central cornea evoked a proliferative response within the cornea but not the limbus (25). They are nonetheless congruent with our recent findings, which demonstrated proliferation of progenitor cells in the limbal margin and subsequent egress of daughter cells into the injury site after inflicting a 2 mm centrally located limbal-sparing wound (6). In larger (~3 mm) wounds, such that the epithelium up to and beyond the limbus is destroyed, the cornea becomes enveloped by an epithelium that invades from the conjunctiva (26); these observations further support the importance of the limbus as a physical barrier and SC reservoir for the cornea. Other circumstantial evidence in favor of the CESC hypothesis includes the ability of human central corneal epithelia to generate $p63^+$ clonogenic spheres, albeit with less potency than those from the limbus (27), and the capacity of corneal epithelial wounds to heal without limbal input (15, 19). Another study showed that 66% of rabbit corneas were maintained in a healthy state during the 6-mo period after surgically removing the limbus (11). The authors suggested that TACs within basal corneal epithelia maintained tissue integrity over this period, but after 2 subsequent rounds of limbal peritomy, the outcome decreased to 33%. Although these observations suggest that SCs persist in the central cornea, they are at odds with our results (*SI Appendix*, Fig. S1).

An alternative proposition is that differentiated cells can revert to a stem-like state. After surgically debriding the limbus of a green fluorescent protein (GFP)-biosensor mouse, Nasser and colleagues observed that cornea-committed $K12^+$ epithelia could de-differentiate into $K15^+$ LESCs. These cells were able to repopulate the limbal SC reservoir and reformed a tissue boundary, then generated daughter cells that migrated centripetally to renew the corneal epithelium (17). In order to achieve these remarkable feats, cells would need to travel "backward," revert from a committed program, implant into the SC niche, which may have been severely damaged by the original injury, then function as bona fide SCs by spawning daughter cells with the ability to clonally expand and move "forward" to maintain tissue mass for 4-mo. To our knowledge, only one other study has provided evidence for this phenomenon. Wang and coworkers suggested that basal corneal epithelia acquired the ability to revert into cells that expressed LESC markers in patients that had undergone surgical procedures that incurred a corneal wound (28). An explanation given for the switch in phenotype and function was alterations in the basement membrane composition upon wounding.

Using a similar model where the entire limbus and peripheral cornea was debrided (otherwise referred to as a type III wound), we observed the development of clinicopathological features of LSCD (26), including corneal opacification, circumferential angiogenesis, and the appearance of goblet cells within the injury zone (*SI Appendix*, Fig. S1 *B–D*). Secondly, the intact central corneal epithelial island either remained as a conglomerate of $K12^+$ cells, it became fragmented (*SI Appendix*, Fig. S1*D*), or it disappeared (*SI Appendix*, Fig. S1*E*) and was eventually replaced by centripetally invading conjunctival epithelia. These observations, although acquired over a relatively short time frame, suggest that the central epithelium cannot support the cornea in the absence of the limbus and eventually succumbs to conjunctivalization (*SI Appendix*, Fig. S1*F*). Unfortunately, we could not rely on our computational model to predict events that transpire in vivo using this wounding regime, because among other parameters, it is reliant on SCs being present within an intact limbus.

Irrespective of the speed or direction of clonal migration, the other curiosity we observed was that during the healing of limbal-sparing

annular wounds, clones did not always reconnect, i.e., they remained detached from their original colony and therefore generated a distorted striping pattern (Fig. 2*E*). These results have been substantiated in other transgenic models (10, 29) and suggests that clones do not necessarily travel on predestined paths to reach their final destination. Importantly, the distorted streaks disappeared during long-term monitoring (Fig. 3), further supporting the notion that central epithelia are eventually replaced by limbal-derived cells.

Our results have far-reaching implications in the realm of cell therapies and drug discovery for patients with severe corneal disease in need of SC replacement and those requiring wound-healing factors to repair their corneal epithelial defects. Herein, we visualized and quantified the contribution of central vs. peripheral/limbal epithelia during annular wound healing by intravital imaging, through an organ culture system, and via computational modeling. Our results verify the contribution of $K14^+$ limbal-derived SCs and their early progeny in playing a vital role in this process and in maintaining a healthy cornea, while central corneal epithelia contribute minimally.

Materials and Methods

Mice. $K14CreER^{T2}$-Confetti mice ($n = 15$) and age-matched WT C57BL/6 ($n = 19$) were housed under pathogen-free conditions and fed standard chow (Gordon's Specialty Feeds). All studies were conducted in accordance with the Australian Code of Practice for the Care and Use of Animals for Scientific Purposes. All procedures were approved by the UNSW Animal Care and Ethics Committee (Approval No. 17/81A).

Induction of the Brainbow Transgene. $K14CreER^{T2}$-Confetti mice harbor a tamoxifen-inducible, K14-promotor-driven Cre recombinase (30) which randomly recombines 2 reversible fluorescent reporter constructs containing 4 fluorescent proteins engineered into the Brainbow 2.1 cassette (31). This results in the stable expression of 1 of 10 distinguishable colors in a K14-defined cell that is inherited by a daughter cell in homozygous mice, enabling long-term lineage tracing (3, 5, 6, 32).

Six-week-old male and female transgenic mice (heterozygous for $K14CreER^{T2}$ and homozygous for Confetti) were injected intraperitoneal (IP) with 50 μg/g of body weight of tamoxifen (Sigma-Aldrich) dissolved in 10% ethanol and 90% olive oil (Sigma-Aldrich) over 3 consecutive days; for experimentation, they were used at 1-wk or 30-wk posttamoxifen administration. This schedule provided ample time for fluorescent patches (i.e., underdeveloped clones typically found in the central cornea) to form and multicolored streaks (i.e., mature clones) to arise from marginally located $K14^+$ LESCs.

Corneal Epithelial Debridement Wounds. Mice were anesthetized by an IP injection of 100 μg/g ketamine (Provet) and 10 μg/g xylazine (Sigma-Aldrich), after which they were placed under an OPMI pico surgical microscope (Carl Zeiss). Epithelial debridement was performed with an Algerbrush II (Katena Products, Inc.) as previously described (6, 33). Injuries differing in size and location were created. The first was inflicted by removing the epithelium between 2 regions of cornea demarcated with a 1.5 and 2.5 mm trephine (~0.5/0.5 mm wide; otherwise termed a type I wound); the second with a 1.5 and 3 mm trephine (~0.75/0.75 mm wide; otherwise termed a type II wound) (KAI Medical), leaving limbal border and a central island of corneal epithelium intact. Because young and old mice were used throughout the study, we rationalized that wounds of slightly different widths were needed, i.e., proportional to eye size and relative to mouse age. The rationale for using mice at the 2 different ages was to determine the ideal chase period in order to visualize whether the uninjured central island was remodeled with newly generated peripheral epithelia. The third injury model (termed a type III wound) was created by demarcating the cornea with a 1.5 mm trephine after which the limbal and peripheral epithelium was removed, leaving behind an intact central island of cells. After wounding, the right eye was copiously rinsed with saline to remove any cell debris; the left eye was uninjured and acted as the internal control. Saline was instilled in both eyes to maintain hydration while mice recovered.

Histological Assessment. Mice were euthanized by cervical dislocation at specific time points postwounding. Eyes were enucleated, fixed in 10% neutral buffered formalin overnight at room temperature (RT), then placed in 70% ethanol. Corneas were procured from intact globes and bisected prior to embedding in agarose, then paraffin; this ensured correct orientation relative to the wound. Tissue sections (4 μm) were cut, stained with PAS, and imaged as previously described (6).

Measuring Clonal Migration and Wound Closure by Intravital Microscopy. Anesthetized Confetti and WT mice were placed under a 3i VIVO fluorescence microscope (Intelligent Imaging Innovations), and wide-field images were acquired using 4 filters compatible for cyan fluorescent protein (CFP), GFP, YFP, and red fluorescent protein (RFP) to record the status of the ocular surface prior to wounding; CFP 458 nm excitation, 464 to 495 nm emission; GFP 488 nm excitation, 497 to 510 nm emission; YFP 514 nm excitation, 517 to 540 nm emission; RFP 561 nm excitation, 575 to 654 nm emission. A droplet (25 μL) of 0.1% sodium fluorescein (Minims, iNova Pharmaceuticals) was instilled for 5 s, each eye was rinsed with 5 mL of phosphate buffered saline (PBS), then corneas were imaged again. At selected time points, corneas were assessed by intravital microscopy using a 2.5×/0.085 detection lens, images were taken and processed using SlideBook v.6 (3i Intelligent Imaging Innovations, https://www.intelligent-imaging.com) and ImageJ software (NIH, https://imagej.nih.gov/ij) (34, 35). Clone number and clone size were quantified in the central (center-to-875 μm), intermediate (875 μm-to-1250 μm), and peripheral (1250 μm-to-eyelid edge) zones from 0 h to 8-wk postinjury. In brief, image registration was performed to ensure alignment of all micrographs, then pixels corresponding to YFP fluorescence were used for subsequent analyses. Wound closure rate was estimated from measurements taken after applying fluorescein. Clonal migration in Confetti mice was estimated by measuring the length of 5 or more limbal-derived streaks of each color over time, and the rate was expressed in μm/h (3, 5, 6, 32).

Light-Sheet and Confocal Microscopy. Confetti mice were euthanized at designated time points postwounding, eyes were enucleated, fixed in 4% paraformaldehyde overnight at 4 °C, and placed in PBS prior to experimentation. Corneas were extracted, extraneous tissues (lens, iris, retina, and ocular muscles) were removed and imaged by light-sheet microscopy (Zeiss Lightsheet Z.1; Carl Zeiss) using a 5×/0.16 detection lens and 5×/0.1 illumination lens, and confocal fluorescence microscopy (Zeiss LSM 780; Carl Zeiss) with a 20×/0.8 or 100×/1.4 detection lens. The 4 fluorescent protein signatures were collected sequentially as follows; CFP 445 nm excitation, 460 to 500 nm emission; GFP 488 nm excitation, 505 to 545 nm emission; YFP 514 nm excitation, 525 to 545 nm emission; RFP 561 nm excitation, 575 to 654 nm emission with light-sheet microscopy, and CFP 458 nm excitation, 455 to 499 nm emission; GFP 488 nm excitation, 490 to 508 nm emission; YFP 514 nm excitation, 517 to 544 nm emission; RFP 561 nm excitation, 579 to 659 nm emission with confocal microscopy. For light-sheet microscopy, whole Confetti corneas were embedded in 1.5% agarose and the tissue was block immersed in PBS within the microscope's imaging chamber. Z-stack images were collected with an optimal sectioning step of 4.35 μm (proximally 550 slices), merged using a maximum intensity projection, and analyzed with Arivis Vision4D (Arivis). After acquiring images, several radial incisions were made on the same specimens to facilitate flat mounting. Corneas were placed epithelium side-down on glass slides, mounted in ProLong Gold anti-fade reagent containing DAPI (Life Technologies), weighted overnight to facilitate flattening, and imaged using a Zeiss 780 confocal microscope (Carl Zeiss). To capture the entire sample, 121 frames were merged into a single 11 × 11 tiled image. Z-stack images were collected, merged using a maximum intensity projection with Zen (Carl Zeiss), and analyzed with ImageJ software. The number of fluorescent stripes was determined by manually counting each as they emerged from limbal margin. Clone width at the periphery was estimated (using a scale bar as a reference) from at least 10 fluorescent streaks comprising YFP and RFP (3, 6).

Cell Proliferation Using BrdU Incorporation. To determine the level of cell proliferation, WT mice were wounded (as described above) then injected IP with BrdU (100 μg/g of body weight) (Sigma-Aldrich) at 16 h postwounding. After 4 h, mice were euthanized, and eyes were enucleated and fixed in 4% paraformaldehyde (PFA) overnight at 4 °C. Corneas were dissected and stained for BrdU as previously described (3, 6, 36). In brief, corneas were treated with 2N HCl for 20 min at RT, washed 4 times (5 min each) in PBS at RT, blocked in 20% goat serum diluted in PBS containing 2% bovine serum albumin (BSA) and 0.1% Triton X-100 (PBS-BT) overnight at 4 °C, then reacted with a rat anti-BrdU antibody (5 μg/mL; ab6326; Abcam) in PBS-BT for 48 h at 4 °C. Corneas were washed thrice (20 min each) in PBS-BT at RT, incubated with a goat anti-rat Alexa-$Fluor^{633}$-conjugated secondary Ab (5 μg/mL; Life Technologies) at 4 °C, counterstained with Hoechst 33342 (1 μg/mL; Life Technologies), flat-mounted in ProLong Gold anti-fade reagent, and scanned by confocal microscopy as described above. Next, $BrdU^+$ cells were counted over unlabeled cells, and a labeling index generated. To achieve this, a grid with 4 equally distant concentric rings was drawn over each cornea, and zones were numbered accordingly; 1 (limbus), 2 (peripheral cornea), 3 (paracentral), and 4 (central).

$BrdU^+$ basal epithelia within zone 1 and between zones 3 and 4 were counted in each of 4 randomly selected regions that measured 425 × 425 μm in area.

Monitoring Corneal Wound Resolution in Organ Culture. Confetti mice were wounded as described above, animals were euthanized, and eyes immediately enucleated. Paired (wounded and intact) globes were embedded in sterile 1.5% agarose and placed within the microscope's imaging/incubation chamber, which was set to 37 °C and 5% CO_2 prior to immersion in defined keratinocyte serum-free media (dKSFM; Gibco) containing 50 nM recombinant human epidermal growth factor (Peprotech), 500 nM Cholera Toxin (List Biological Labs, Inc.), and 100 U/mL Penicillin-Streptomycin (Gibco) (6). Eyes were imaged every 2 h over 48 h by light-sheet microscopy (Zeiss Lightsheet Z.1) using a 5×/0.16 detection lens and 5×/0.1 illumination lens as described above.

Clone Migration by Spatiotemporal Image Correlation Spectroscopy in Organ-Cultured Corneas. As an alternative and more accurate means of measuring cell movement, STICS (37–39) was applied on a series of 2-dimensional (2D) maximum intensity projections of 3D image stacks that were acquired via light-sheet microscopy at different time points postinjury in ex vivo organ-cultured murine corneas as previously described (6). The raw data consisted of a temporal sequence (i.e., time point per 2 h) of Z-stacks from corneas imaged through a 5×/0.16 detection lens and 5×/0.1 illumination lens as described above (pixel size 2.28 μm).

Computational Model of Corneal Epithelial Wound Healing. The agent-based computational model was used to investigate the role that population pressure-driven motility plays in corneal wounding and repair and to compare spatial distributions of clonally related cells in corneas, following cases of no wounding and annular wounding of the peripheral cornea. It was based on a previous model (5, 40) and modified to incorporate regions in which epithelial cells were removed by wounding as previously described (6), except that, in this case, the wound made was annular. Briefly, basal corneal epithelial cells are represented as Voronoi tessellations in a circular shape bounded by SCs. Epithelial cells have a limited replicative lifespan and are removed from the cell sheet after having undergone a number of cell divisions; neighboring cells then immediately occupy the vacated space. Cells measure population density locally by determining the number of neighbors and move from directions of high pressure toward low pressure. SCs can undergo an unlimited number of replications that give rise to one epithelial cell and one replacement stem cell. When a stem cell dies, it is replaced by the replication of a neighboring stem cell. Wounds are created by substituting epithelial cells with "blank" cells, which produce less pressure than epithelial cells and do not replicate. A detailed description of the model is included in Supplementary Information in standard ODD (Overview, Design concepts, and Details) format (6, 40).

Statistical Analyses. Data are presented as mean ± SD (n = sample size). Unpaired 2-tailed Welch's t test with unequal variance and ANOVA with Sidak's or Tukey's multiple comparisons was used to compare wound closure between WT and Confetti mice, and the velocity of $K14^+$ clonal migration, clone number and streak width between wounded and contralateral control eyes. Two-way ANOVA with Tukey's or Dunnett's multiple comparisons test was used to compare in vivo clone number and size among central, intermediate, and peripheral zones, respectively. A P value < 0.05 was considered statistically significant. All statistical analyses were performed using GraphPad Prism 7.

Details of slit-lamp biomicroscopy, immunofluorescence, and PAS staining for *SI Appendix*, Fig. S1 are provided in *SI Appendix, Supplementary Materials and Methods*. All data used for the study are within the manuscript and *SI Appendix*. Readers will be able to access MATLAB and code for STICS and computational model by directly contacting the corresponding author.

ACKNOWLEDGMENTS. This work was supported by grants from the Australian National Health and Medical Research Council (APP1101078 and APP1156944), Stem Cells Australia, and the Australian Research Council (SR1101002) to N.D.G.

1. N. Di Girolamo *et al*., Tracing the fate of limbal epithelial progenitor cells in the murine cornea. *Stem Cells* **33**, 157–169 (2015).
2. R. A. Thoft, J. Friend, The X, Y, Z hypothesis of corneal epithelial maintenance. *Invest. Ophthalmol. Vis. Sci.* **24**, 1442–1443 (1983).
3. A. Richardson *et al*., Keratin-14-positive precursor cells spawn a population of migratory corneal epithelia that maintain tissue mass throughout life. *Stem Cell Rep.* **9**, 1081–1096 (2017).
4. M. S. Lehrer, T.-T. Sun, R. M. Lavker, Strategies of epithelial repair: Modulation of stem cell and transit amplifying cell proliferation. *J. Cell Sci.* **111**, 2867–2875 (1998).
5. E. P. Lobo *et al*., Self-organized centripetal movement of corneal epithelium in the absence of external cues. *Nat. Commun.* **7**, 12388 (2016).
6. M. Park *et al*., Visualizing the contribution of keratin-14+ limbal epithelial precursors in corneal wound healing. *Stem Cell Rep.* **12**, 14–28 (2019).
7. J. Lamprecht, Symmetric and asymmetric cell division in rat corneal epithelium. *Cell Tissue Kinet.* **23**, 203–216 (1990).
8. D. C. Beebe, B. R. Masters, Cell lineage and the differentiation of corneal epithelial cells. *Invest. Ophthalmol. Vis. Sci.* **37**, 1815–1825 (1996).
9. F. Castro-Muñozledo, E. Gómez-Flores, Challenges to the study of asymmetric cell division in corneal and limbal epithelia. *Exp. Eye Res.* **92**, 4–9 (2011).
10. R. L. Mort, T. Ramaesh, D. A. Kleinjan, S. D. Morley, J. D. West, Mosaic analysis of stem cell function and wound healing in the mouse corneal epithelium. *BMC Dev. Biol.* **9**, 4 (2009).
11. A. J. Huang, S. C. Tseng, Corneal epithelial wound healing in the absence of limbal epithelium. *Invest. Ophthalmol. Vis. Sci.* **32**, 96–105 (1991).
12. M. T. Budak *et al*., Ocular surface epithelia contain ABCG2-dependent side population cells exhibiting features associated with stem cells. *J. Cell Sci.* **118**, 1715–1724 (2005).
13. T. Umemoto *et al*., Rat limbal epithelial side population cells exhibit a distinct expression of stem cell markers that are lacking in side population cells from the central cornea. *FEBS Lett.* **579**, 6569–6574 (2005).
14. H. S. Dua, A. Miri, T. Alomar, A. M. Yeung, D. G. Said, The role of limbal stem cells in corneal epithelial maintenance: Testing the dogma. *Ophthalmology* **116**, 856–863 (2009).
15. F. Majo, A. Rochat, M. Nicolas, G. A. Jaoudé, Y. Barrandon, Oligopotent stem cells are distributed throughout the mammalian ocular surface. *Nature* **456**, 250–254 (2008).
16. T.-T. Sun, S. C. Tseng, R. M. Lavker, Location of corneal epithelial stem cells. *Nature* **463**, E10–E11 (2010).
17. W. Nasser *et al*., Corneal-committed cells restore the stem cell pool and tissue boundary following injury. *Cell Rep.* **22**, 323–331 (2018).
18. A. Amitai-Lange *et al*., Lineage tracing of stem and progenitor cells of the murine corneal epithelium. *Stem Cells* **33**, 230–239 (2015).
19. C. Y. Chang, C. R. Green, C. N. McGhee, T. Sherwin, Acute wound healing in the human central corneal epithelium appears to be independent of limbal stem cell influence. *Invest. Ophthalmol. Vis. Sci.* **49**, 5279–5286 (2008).
20. W. M. Townsend, The limbal palisades of Vogt. *Trans. Am. Ophthalmol. Soc.* **89**, 721–756 (1991).
21. G. Cotsarelis, S. Z. Cheng, G. Dong, T. T. Sun, R. M. Lavker, Existence of slow-cycling limbal epithelial basal cells that can be preferentially stimulated to proliferate: Implications on epithelial stem cells. *Cell* **57**, 201–209 (1989).
22. A. Schermer, S. Galvin, T.-T. Sun, Differentiation-related expression of a major 64K corneal keratin in vivo and in culture suggests limbal location of corneal epithelial stem cells. *J. Cell Biol.* **103**, 49–62 (1986).
23. J. D. West, N. J. Dorà, J. M. Collinson, Evaluating alternative stem cell hypotheses for adult corneal epithelial maintenance. *World J. Stem Cells* **7**, 281–299 (2015).
24. Y.-L. Bi, F. Bock, Q. Zhou, C. Cursiefen, Central corneal epithelium self-healing after ring-shaped glycerin-cryopreserved lamellar keratoplasty in Terrien marginal degeneration. *Int. J. Ophthalmol.* **6**, 251–252 (2013).
25. K. U. Sandvig, E. Haaskjold, R. Bjerknes, S. B. Refsum, K. Kravik, Cell kinetics of conjunctival and corneal epithelium during regeneration of different-sized corneal epithelial defects. *Acta Ophthalmol. (Copenh.)* **72**, 43–48 (1994).
26. A. Richardson, M. Park, S. L. Watson, D. Wakefield, N. Di Girolamo, Visualizing the fate of transplanted K14-confetti corneal epithelia in a mouse model of limbal stem cell deficiency. *Invest. Ophthalmol. Vis. Sci.* **59**, 1630–1640 (2018).
27. C.-Y. A. Chang, J. J. McGhee, C. R. Green, T. Sherwin, Comparison of stem cell properties in cell populations isolated from human central and limbal corneal epithelium. *Cornea* **30**, 1155–1162 (2011).
28. I.-J. Wang *et al*., Changes in corneal basal epithelial phenotypes in an altered basement membrane. *PLoS One* **6**, e14537 (2011).
29. Y. Hayashi, N. Watanabe, Y. Ohashi, The "replacement hypothesis": Corneal stem cell origin epithelia are replaced by limbal stem cell origin epithelia in mouse cornea during maturation. *Cornea* **31** (suppl. 1), S68–S73 (2012).
30. A. K. Indra *et al*., Temporally controlled targeted somatic mutagenesis in embryonic surface ectoderm and fetal epidermal keratinocytes unveils two distinct developmental functions of BRG1 in limb morphogenesis and skin barrier formation. *Development* **132**, 4533–4544 (2005).
31. J. Livet *et al*., Transgenic strategies for combinatorial expression of fluorescent proteins in the nervous system. *Nature* **450**, 56–62 (2007).
32. N. Di Girolamo, Moving epithelia: Tracking the fate of mammalian limbal epithelial stem cells. *Prog. Retin. Eye Res.* **48**, 203–225 (2015).
33. M. F. Chan, Z. Werb, Animal models of corneal injury. *Bio Protoc.* **5**, e1516 (2015).
34. M. D. Abràmoff, P. J. Magalhães, S. J. Ram, Image processing with ImageJ. *Biophoton. Int.* **11**, 36–42 (2004).
35. A. Cruzat *et al*., Inflammation and the nervous system: The connection in the cornea in patients with infectious keratitis. *Invest. Ophthalmol. Vis. Sci.* **52**, 5136–5143 (2011).
36. A. Pajoohesh-Ganji, S. Pal-Ghosh, S. J. Simmens, M. A. Stepp, Integrins in slow-cycling corneal epithelial cells at the limbus in the mouse. *Stem Cells* **24**, 1075–1086 (2006).
37. T. Toplak *et al*., STICCS reveals matrix-dependent adhesion slipping and gripping in migrating cells. *Biophys. J.* **103**, 1672–1682 (2012).
38. M. B. Meddens *et al*., Actomyosin-dependent dynamic spatial patterns of cytoskeletal components drive mesoscale podosome organization. *Nat. Commun.* **7**, 13127 (2016).
39. G. W. Ashdown *et al*., Live-cell super-resolution reveals F-actin and plasma membrane dynamics at the T cell synapse. *Biophys. J.* **112**, 1703–1713 (2017).
40. V. Grimm *et al*., The ODD protocol: A review and first update. *Ecol. Modell.* **221**, 2760–2768 (2010).